Aerodynamics of a highly cambered circular arc aerofoil : experimental investigations

Richard G.J. Flay, A Piard, Patrick Bot

AERODYNAMICS OF A HIGHLY CAMBERED CIRCULAR ARC AEROFOIL: EXPERIMENTAL INVESTIGATIONS

R.G.J. Flay, A. Piard, University of Auckland, New Zealand, r.flay@auckland.ac.nz, apia386@aucklanduni.ac.nz,
P. Bot, Ecole Navale - IRENav, France, patrick.bot@ecole-navale.fr

While the aerodynamics of upwind sails are relatively well understood, flows past downwind sails are still very challenging. Indeed, downwind sails which can be considered as highly cambered thin wing profiles, are well known for their massive separations and complex wake flows. Therefore the aim of this study was to examine a very simple highly curved thin wing profile in order to elucidate features of real flow behaviours past such sails. Therefore, a two-dimensional thin circular arc has been investigated. The studied model had a camber of 21 - 22% comparable to downwind sails. The wind tunnel pressure measurements have enabled us to understand why the sudden transition in the lift force exists at low incidences but not at higher incidences. At low incidences the flow stagnates on the top face and a laminar boundary layer develops first. If the Reynolds number is too low, the laminar boundary layer is not able to transition to turbulent. This laminar boundary layer separates very early leading to low lift and high drag. However, when the Reynolds number is high enough, the boundary layer transitions to turbulent creating a laminar separation bubble. This more robust boundary layer can withstand the adverse pressure gradient and stay attached much longer, creating a sudden significant increase in lift and a drop in drag. At high incidences, a leading edge bubble forces the flow to transition to turbulent. Therefore, the boundary layer is fully turbulent irrespective of the Reynolds number and a unique flow regime exists at these high incidences.

1 INTRODUCTION

While the aerodynamics of upwind sails is well understood, flows past downwind sails are still very challenging. Indeed, downwind sails with their highly cambered thin profiles are known for their massive separations and complex wake properties. The aim of this study is to isolate a simple as possible geometry in order to model the flow behaviours past such sails. Therefore, a two-dimensional thin circular arc was investigated.

In previous publications all the experiments performed on the 2D profiles have only provided lift and drag as global forces. But because different pressure profiles can generate the same global forces, knowing the local pressure distributions is crucial for CFD code validations. To assist in remedying this situation, the paper discusses an extensive set of pressure measurements on a 2D wing using the University of Auckland wind tunnel.

2 LITERATURE REVIEW

To provide a framework for understanding the aerodynamics of highly cambered wings, it is firstly necessary to review some basic aerodynamics concerning transition and separation before considering some of the previous work on circular arc wings.

According to White [1], boundary layer transition on a flat plate is normally assumed to occur at around 5×10^5, but by polishing the surface and having very smooth onset flow, transition may be delayed until $Re = 3 \times 10^6$. On the other hand, if the freestream flow is turbulent and the surface is rough, transition may occur much earlier. Pressure gradients in the flow also have a significant effect. Lissaman [2] has shown that for a range of smooth aerofoils transition occurs at approximately 10^5 and causes a sudden increase in lift. Fig. 1 shows the sudden increase in lift to drag ratio during this process. At the higher Reynolds numbers (Re), separation does not occur so early on the upper suction surface, so larger suctions can occur, thus leading to higher lift coefficients.

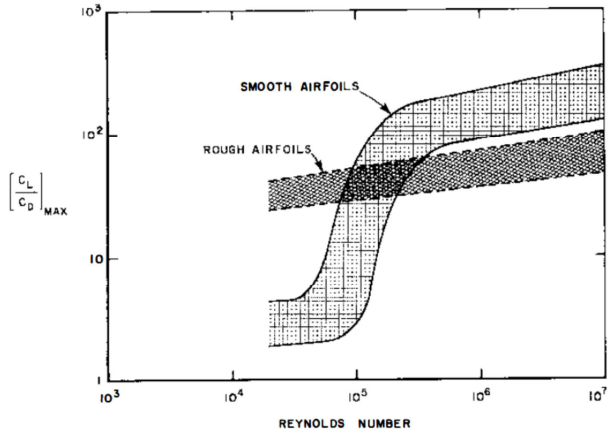

Figure 1: Reynolds number influence on rough and smooth aerofoils, Lissaman [2]

On an aerofoil, depending on the conditions (aerofoil shape, angle of attack, Reynolds number etc.) a laminar boundary layer when it separates from the foil due to an adverse pressure gradient that is too strong will transition to a turbulent flow and either remain detached or reattach downstream to the foil. The latter is known as a “laminar separation bubble” [3]. Fig. 2 illustrates the various regions of a laminar separation bubble.

McArthur [4] explains that the laminar separated shear flow is highly unstable and transitions to a turbulent separated shear flow. This turbulence then allows the boundary layer to re-energise by transporting momentum from the free-stream to the surface. If the turbulent boundary layer gains enough energy in this process to overcome the adverse pressure gradient, the flow eventually reattaches to the surface.

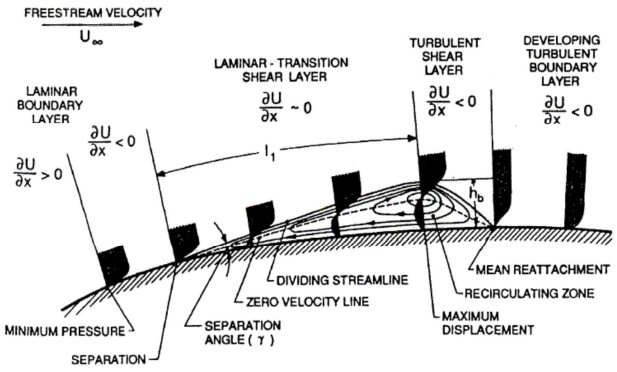

Figure 2: Illustration of a laminar separation bubble [3]

Speranza [5] describes how the laminar separation bubble affects the pressure distribution on aerofoils. By displacing the shear layer away from the surface, the laminar separation bubble acts as a local shape modification of the foil. Therefore, the suction pressure remains almost constant on this area creating a plateau in terms of *Cp* distribution. Fig. 3 illustrates how a laminar separation bubble can be identified on the upper surface of a classical aerofoil.

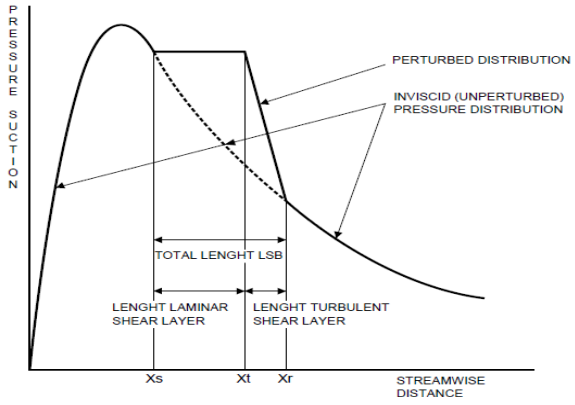

Figure 3: Laminar separation bubble induced pressure perturbation [5]

One of the earliest works on highly cambered profiles was done by Bruining [6] at Delft University of Technology. Wind tunnel tests of curved thin plates were performed mostly to predict the best mast position relative to the main sail. However, the models had only 5% to 10% camber and Reynolds numbers of only 60,000 and 100,000 were investigated.

From previous work on 3D downwind sails, and because of the complexity of such flows, Collie, Jackson and Gerristen [7] decided to study the simpler case of a thin circular arc. For this they examined the flow behaviour on a simplified 2D downwind sail section so as to get accurate data from wind tunnel experiments. They used a rigid, 24.7% cambered, 319 mm long (chord-wise) model. Figure 4 from [8] illustrates the flow behaviour past such highly cambered profiles.

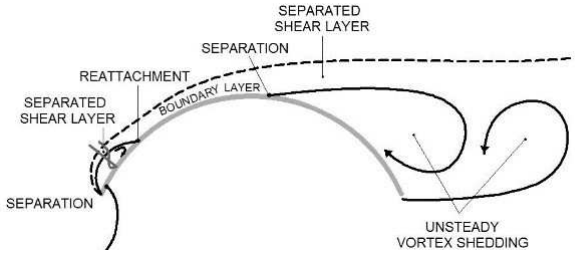

Figure 4: 2D downwind sail flow [8]

In the testing, while the leading edge bubble was shown to be 2D, the wake was highly influenced by the wind tunnel walls as the model span was only 1.4 times its chord. More results are available in Collie's PhD thesis [9] that describes a rigid 25% camber model with a high aspect ratio of 18:1 tested at a Reynolds number of 3.77 x 10^5. Results for angles of attack from -5° to 30° were studied, even though they are outside the range used for downwind sails.

The Sailing Fluids collaboration involving the Yacht Research Unit at the University of Auckland, Newcastle University, IRENav in France and the University of Edinburgh also decided to examine a circular arc wing as a simplification of the section of a spinnaker at about half-height. CFD analysis was carried out at Newcastle University and the University of Edinburgh, water tunnel experiments at Ecole Navale, and wind tunnel measurements at the Yacht Research Unit.

The first experimental water tunnel work was carried out by Lebret [10, 11]. Lebret's 2D model was cut from a 3 mm thick steel cylinder with an outer radius of 50 mm. The chord is 74.45 mm, the span 191.5 mm, the leading and trailing edge angles are 48.12°, the camber is 22.3% and the camber aspect ratio span/chord is 2.57. There was a 0.25 mm gap at either end so that the model did not touch the sides of the water tunnel. This investigation used a force balance to measure lift, drag and pitching moment, as well as particle image velocimetry (PIV). The velocity field was very uniform in the vicinity of the model. The turbulence intensity was measured by LDV and determined to be about 2.3% at the model location. In this work an unexpected result occurred, where the lift force reversed sign at a particular Reynolds number when the wing was placed at zero angle of attack.

Lombardi [12] continued Lebret's work and used the PIV measurement system to generate velocity fields for each configuration. This allowed him to have a much better understanding of how was the flow actually behaved. A

similar critical Reynolds number of around 2.0×10^5 was determined for the 0° angle of attack configuration. While the lift coefficient was seen to suddenly jump from -0.45 to +0.6, the drag coefficient was also seen to show a significant drop from 0.15 to 0.09 at the critical Reynolds number.

Using the flow field visualisation available from the PIV, Lombardi was able to explain what was happening. At Reynolds numbers lower than critical, it could be seen that the flow separates from the suction side of the wing at mid-chord. There is a corresponding large wake, which is directed slightly upwards, as expected from the negative lift. However, at Reynolds numbers above the lift crisis the flow separates much further downstream, producing a wake that is much smaller and directed downwards, again as expected for the positive lift in this region of Re.

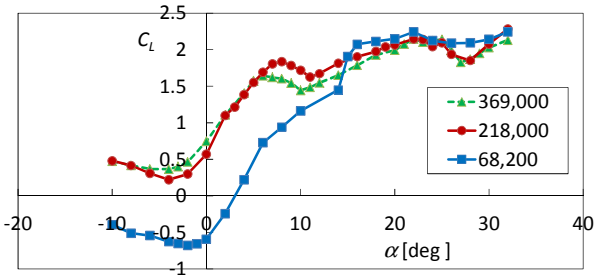

Figure 5 Lift coefficient versus angle of attack for sub- and super-critical Reynolds numbers [12]

The significant differences in lift and drag coefficients for Re above and below 2×10^5 can be seen in Fig. 5. Around 10° and 11° for Reynolds numbers of 2.18 x 10^5 and 3.69 x 10^5 respectively, the curve has a local minimum and then rapidly rises again. For Re = 6.82 x 10^4, the curve jumps quickly at an angle of attack of 14°. Martin [13] and Thomas [14] carried out further PIV work in the water tunnel and examined these phenomena by concentrating on the leading edge. It was apparent that a leading edge vortex appeared as the angle of attack was increased slightly in these regions where the lift coefficient increased.

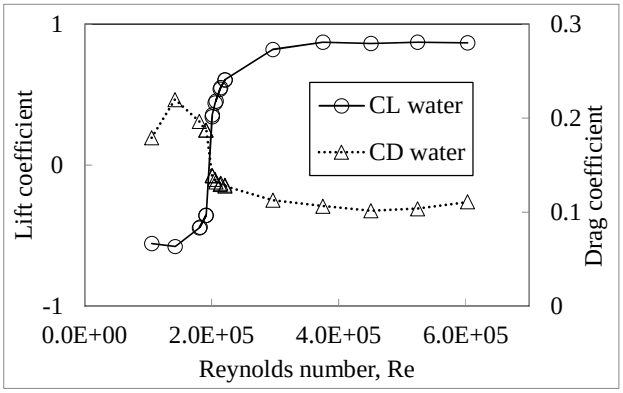

Figure 6: Lift and drag coefficients versus Reynolds number, as measured with a force balance in the water tunnel [15]

The Ecole Navale work from the extensive water tunnel investigations [10–14] is discussed in detail by Bot et al. [15]. This paper gathers together a significant amount of information from a large number of publications and provides evidence for the appearance of a “lift crisis” for flow past non-symmetrical obstacles, in the drag crisis regime. Fig. 6, using data from [15] shows the water tunnel lift and drag coefficient measurements. The PIV images are analysed and the separation on the top surface was found to be at 57% chord for subcritical Reynolds numbers, increasing to 95% for supercritical Reynolds numbers. Wake analysis also showed a deflection upwards at low Re, and downwards above the lift crisis, as expected, given the change in sign of C_L at the lift crisis. These interesting results inspired further numerical studies, and Nava et al. [16] discuss the comparison of LES and RANS simulations with the PIV experimental results from the Ecole Navale water tunnel.

3 WIND TUNNEL PRESSURE STUDY

In addition to the water tunnel work at Ecole Navale, it was decided to undertake pressure measurements on a model of the wing in the large open jet wind tunnel at the University of Auckland. The aim was to size the model so that the Reynolds number test range would envelope the region where the lift crisis occurred. The results of this investigation were written up by Piard in his Master of Yacht Engineering Research Report [17]. The remainder of this paper is mainly focused on discussing and comparing these wind tunnel pressure measurements, which are the first to be obtained on this highly cambered wing.

4 WIND TUNNEL EXPERIMENTAL SET-UP

The wind tunnel was set up in the configuration with the walls contracted so that the open jet for testing was 2.5 m wide and 3.5 m high, with the model located horizontally at the outlet, as shown in Fig. 7.

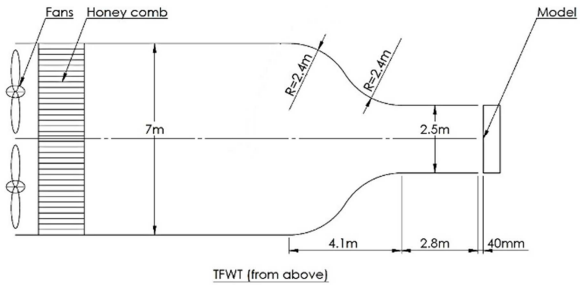

Figure 7: Schematic plan view of model positioned at the outlet of the University of Auckland Wind Tunnel. The jet is 2.5 m wide and of 3.5 m wide.

The wind tunnel model design was aimed at scaling up the water tunnel model chord by a factor of 8, to give a Reynolds number around 2 x 10^5 at an air speed of 5 m/s, which was near the middle of the proposed test speeds of

2 to 10 m/s. The dimensions of the actual model are shown in Fig. 8.

The wind tunnel model changed shape slightly after being glued, and its camber was 21.3%, slightly lower than the target value of 22.3%. The model can be seen in Fig. 9.

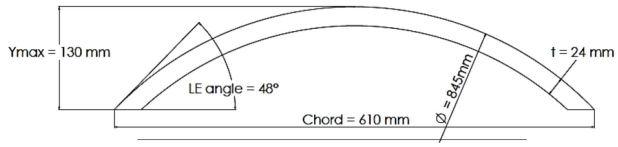

Figure 8: Wind tunnel model sectional dimensions

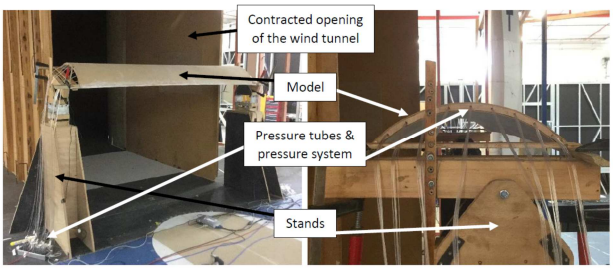

Figure 9: Photographs of the model mounted in the open jet (left), and an end-view of the model mounted on stands.

A total of 81 pressure taps were used on the model. These were concentrated on the top surface near the leading edge, with a lower tapping density further downstream and underneath where the pressure gradients were expected to be much lower. They were angled across the model at 15° and 7° for the upstream and downstream suction surface taps respectively, to ensure that the wake from an upstream tap did not interfere with the pressure measured by a downstream tap. A few taps were positioned laterally across the model at spacings up to 200 mm in order to check on the span-wise uniformity of the pressure distribution. Pressures were sampled for a period of 60 s at a frequency of 100 Hz. The accuracy of the pressure measurements is estimated to be +/- 1 Pa. Pressure coefficients were formed using the dynamic pressure at the model location, and the static pressure of the jet outlet.

Prior flow measurements to establish the flow field in the test region showed that the flow was very 2D in the vicinity of the test region and that the turbulence intensity was around 1% for all test speeds. The pressure distributions were measured for angles of attack ranging from -5° to +25° every 5°. For each angle of attack, tests were carried out at 12 different speeds giving Reynolds numbers in the range 116,000 to 415,000.

5 DISCUSSION OF WIND TUNNEL RESULTS

The rationale behind undertaking the present research into the circular arc wing was to attempt to understand the more complicated flow over 3D sails. Pressure distributions on sails are expected to look rather like the schematic diagram from Viola and Flay [18], reproduced here as Fig. 10. Hence we desire measured pressure distributions from the wing model when set at a normal sailing angle of attack to look similar to those in figure 10.

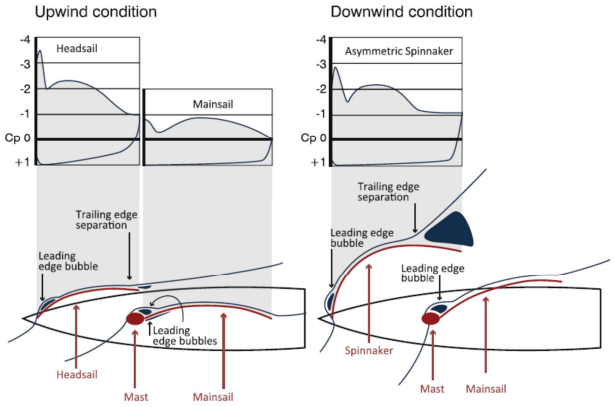

Figure 10 Schematic drawing of the flow and pressures around sails in upwind and downwind conditions [18]

Fig. 11 shows the influence of the Reynolds number at an angle of attack of 20°. The graph displays four different pressure distribution curves: top, bottom, leading edge and trailing edge. The measurements from the two taps located on each of the flat underside surfaces at the leading and trailing edges (see Fig. 8.) are displayed further upstream and downstream respectively, for clarity.

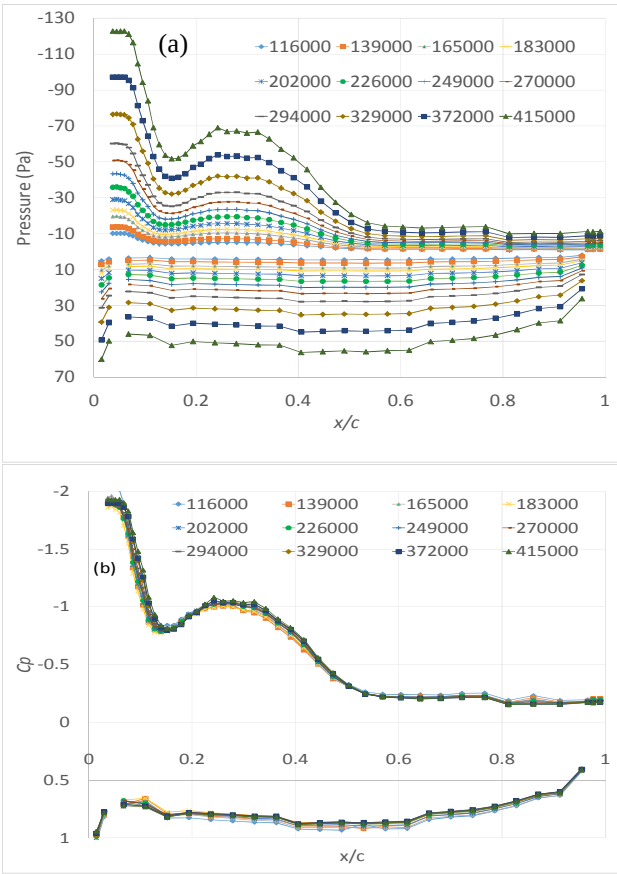

Figure 11 Pressure distributions (a) and corresponding *Cp* distributions (b) for an angle of attack of 20°.

While the pressure distributions increase in magnitude with the Reynolds number, the non-dimensional *Cp* distribution for this angle of attack is clearly independent of Reynolds number. However, the previous work, e.g. Fig. 5 from [12] shows that the independence of the flow regime from Reynolds number was only true for angles of attack greater than 15°. For smaller angles of attack a strong dependency on the Reynolds number was observed in the water tunnel results. Also note that the general features of the pressure distribution in Fig. 11(b) are similar to those presented in Fig. 10, so the 2D wing has aerodynamic features that look similar to those we expect on sails. On the top surface there is a high suction near the leading edge from a small separation bubble, a reduction in suction with a minimum at 15% chord, then an increase due to the curvature of the wing, followed by a constant region aft of 55% where the flow has separated from the wing. As expected, pressures on the lower surface are relatively uniform.

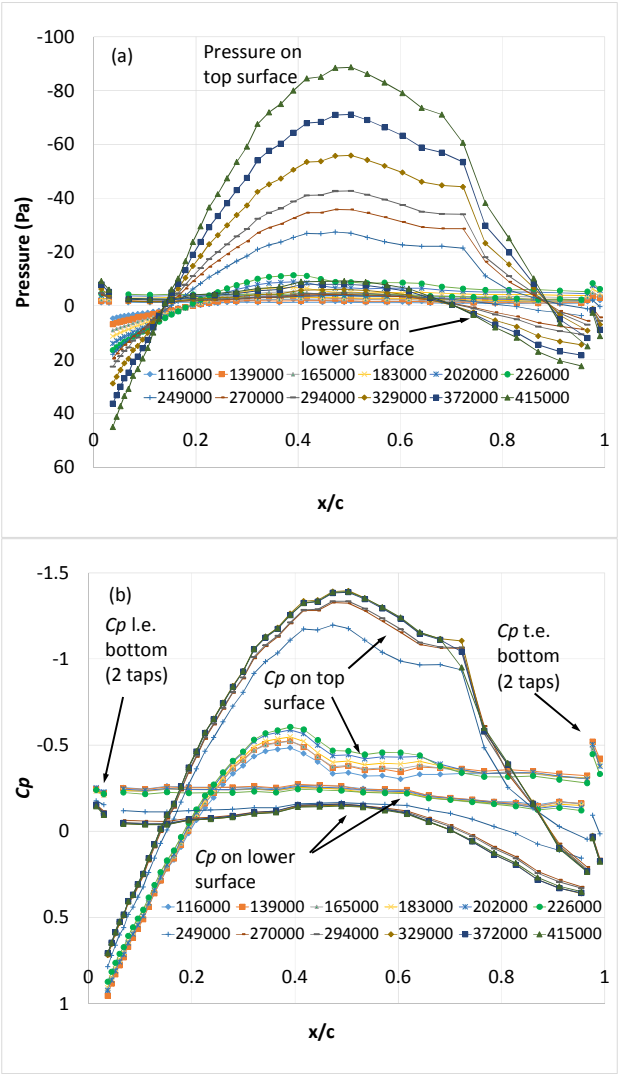

Figure 12 Pressure distributions (a) and corresponding *Cp* distributions (b) for an angle of attack of 0°

Fig. 12 is similar in format to figure 12, but the angle of attack of the wing is 0°. Here it can be seen that the pressure distributions on the upper and lower surfaces can be positive and negative. The pressure distributions do not resemble those that are seen on well-trimmed sails. There is no large suction on the top surface at the leading edge; in fact the pressure is positive there and flexible sails could not take up this shape as they would fold and/or collapse. The water tunnel investigation showed that the lift and drag coefficients had a strong dependency on Reynolds number below about 200,000 for angles of attack in the region of -5° to 10°, and it is evident in these *Cp* results that there is a dramatic change in the shapes of the distributions in the Re region 226,000 to 249,000. For low Re the flow separates at approximately mid-chord, whereas for high Re the suction is much stronger and the flow remains attached for much longer, almost up to the trailing edge. Similar behaviour to that shown in Fig. 12 for 0° was also shown in the measurements at angles of attack of -5° to 10°, whereas the pressure distributions for angles of attack from 15° to 25° showed no Re dependency and were like the curves shown in Figs 11(a,b).

5.1 LIFT AND DRAG BY INTEGRATION

Since the wing model was not connected to a force balance, overall sectional lift and drag were determined by integrating the pressure distribution around the chord. This was done by simply assigning an appropriate area to each pressure tap, and using the orientation of each pressure tap to determine the contribution of the pressure at each location to the lift and drag.

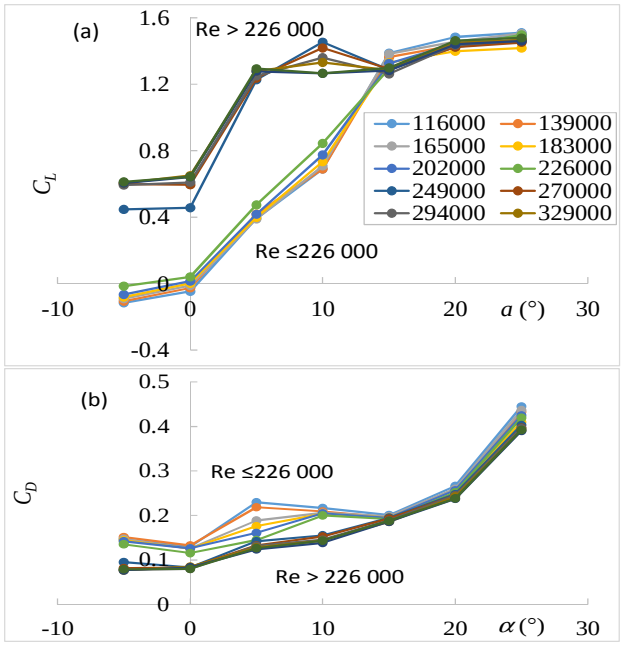

Figure 13 Lift (a) and drag (b) coefficients versus angle of attack for a range of Reynolds numbers.

It should be noted that the drag does not include the skin friction drag, and because of manufacturing

considerations it was not possible to have pressure taps within 20 mm of the leading edge of the wing. Estimates of possible skin friction drag were made using the ITTC formulae for both laminar and turbulent boundary layers. From these calculations it is estimated that the contribution of turbulent skin friction drag may be up to 10% for the results at low incidences, but that it is negligible at high angles. The leading edge region without taps represents only 4% of the total area of the model, and so its potential contribution to experimental errors is relatively small.

Lift and drag coefficients are plotted in Figs. 13(a,b). It is clearly evident that there are two groups of results for angles of attack less than 15° that depend on Re, but that at higher angles the results are grouped together. This is as-expected from the differences shown in the pressure distributions from which the force coefficients have been derived.

For the low Re group, the lift coefficient at zero incidence is near zero, and so it appears in these wind tunnel measurements that at low Re the flow does not see the camber of the profile, but the flow acts like it is a relatively symmetric bluff body. C_L then increases linearly until it merges with the higher Re group of C_L curves at an angle of attack of 15°. The drag coefficient is also higher at low Re than for higher Re at these angles of low incidence.

For the high Re group, the lift at zero angle of attack is high at around 0.6. It then increases to reach a local maximum at α = 10° for 249 000 < Re < 329 000. For still higher Re it reaches a plateau for 5° < α < 15°. Then all the lift curves merge and slowly increase from 15° to 25°.

5.2 EFFECT OF ANGLE OF ATTACK ON LIFT CRISIS OCCURRENCE

Lift and drag coefficients are plotted for each angle of attack as a function of Re in Fig. 14.

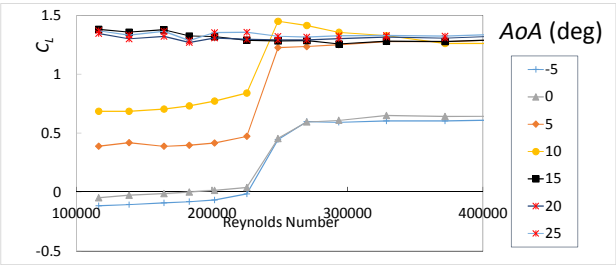

Figure 14: Lift and drag coefficients for each angle of attack versus Re

The transition in C_L is clearly very sharp for angles below 15°, but the low Re flow regime completely disappears for angles greater than 15°. As discussed above, for small angles of attack (α = -5° and 0°) and small Re the flow does not seem to "see" the camber of the profile, producing null to slightly negative lift. But even with a negative angle of attack of -5°, above the transition Re the lift flips to a significantly positive value of C_L = 0.6.

The sudden increase in lift is very similar to the aerofoil transition behaviour [2] shown in Fig. 1. Although not shown, at the same time as when the lift suddenly increases, a noticeable drop in drag is recorded. When transition of the boundary layer on the top surface occurs before the location of laminar separation, the fuller turbulent boundary layer remains attached for longer, thus reducing the width of the wake, and consequently the drag.

The wind tunnel lift and drag coefficient measurements for α = 0° are compared with the measurements described by Bot et al. [15] from the water tunnel in Fig. 15.

Both experiments show similarities in term of lift and drag behaviour, but there are still some differences. Transition occurs a little later in the wind tunnel experiment. This might be because of the difference in free stream turbulence intensities. The wind tunnel mean turbulence intensity was around 1%, whereas it was about 2% in the water tunnel. The free stream turbulence transfers kinetic energy to the boundary layer. Therefore, the higher the free-stream turbulence, the earlier the boundary layer is likely to transition to turbulent.

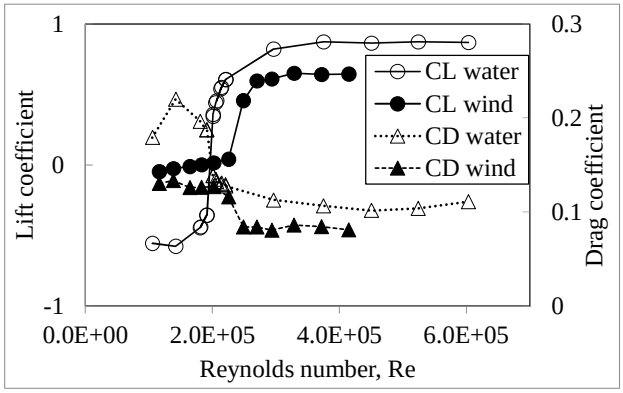

Figure 15: Comparison of lift and drag coefficients versus Reynolds number, as measured with a force balance in the water tunnel, and by pressure integrations in the wind tunnel.

While the measured drag coefficients are almost identical at about 0.1, the lift curves do not reach the same magnitudes. The higher positive lift for high Reynolds numbers in the water tunnel might be due to the higher blockage. The walls of the cavitation tunnel were only 1.0 to 1.3 chords from the model, and thus the acceleration of the fluid around the model and the higher local dynamic pressure of the flow would have increased the lift and drag forces. In the wind tunnel the distance from the model to the top and bottom walls was about 3 times the chord length and so the blockage was

considerably less. Why the lift is so negative at low Re in the water tunnel but is barely negative in the wind tunnel remains unexplained at this stage, but could also be related to the differences in blockage.

The assumption above that the sudden change in flow behaviour is caused by boundary layer transition can be confirmed by studying the wind tunnel pressure distributions. The understanding of why two different flow regimes exist for small angles of attack, but only one regime exists for larger angles of attack can also be explained by looking closely at the *Cp* distributions.

5.3 PRESSURE COEFFICIENT DISTRIBUTIONS

Studying the pressure distributions helps explain why the two flow regimes can exist at low angles of incidence, while only one regime exists at high angles.

In order to make this analysis easier to understand, the *Cp* distributions are divided into three different categories which define three different flow behaviours that are evident:

- Low Reynolds numbers/Low incidences
- High Reynolds numbers/Low incidences
- All Reynolds numbers/High incidences

5.3.1 Low Reynolds Numbers/Low Incidences

In Fig. 17 it can be seen that for small angles of attack (α = -5° and 0°), in addition to a high positive pressure on the first 25% of the upper surface due to the flow stagnating, only a low suction occurs on the lower surface. These pressures give rise to the slightly negative to zero lift experienced for these low angles of attack at low Reynolds numbers. Since the suction on the top surface is very weak and is balanced by the top surface leading edge positive pressure, the sign of the overall lift force on the wing relies heavily on whether the pressure on the bottom surface is positive or negative.

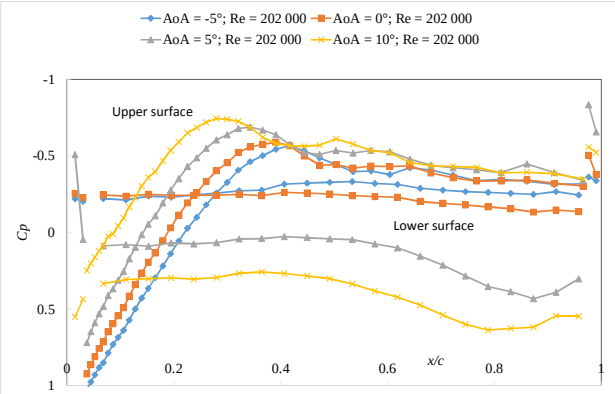

Figure 17 *Cp* distribution for low Re ≤ 226,000 and low $\alpha \leq$ 10° versus *x/c*

These Cp distributions shape are typical of weak laminar boundary layers that have been observed many times on circular cylinders - a weak suction separating very early from the surface.

At zero incidence the flow separates at approximately mid-chord. Increasing the angle of attack causes the adverse pressure gradient on the top surface to increase as well, thus separation occurs even earlier (at *x/c* = 0.45 for 5° and at *x/c* = 0.4 for an angle of 10°).

The stagnation point occurs at *x/c* = 0.045 for α = -5°. Even if the pressure is not known forward of *x/c* ≤ 0.037 where there are no pressure taps on the underside, it is clear that the stagnation point is moving closer and closer to the leading edge with increasing α. The pressure becomes even positive on the bottom of the leading edge for $\alpha \geq$ 5°, which also indicates that the stagnation point is moving closer to the leading edge.

5.3.2 High Reynolds Numbers/Low Incidences

The pressure distributions for high Reynolds numbers are very different from those for low Reynolds numbers as illustrated in Figure 18. The suction on the top face is much stronger both in terms of magnitude and length of attachment. The shape of these pressure distributions are typical of those for laminar boundary layers that are transitioning to turbulent. The fuller turbulent boundary layer is able to stay attached for much longer than a laminar boundary layer.

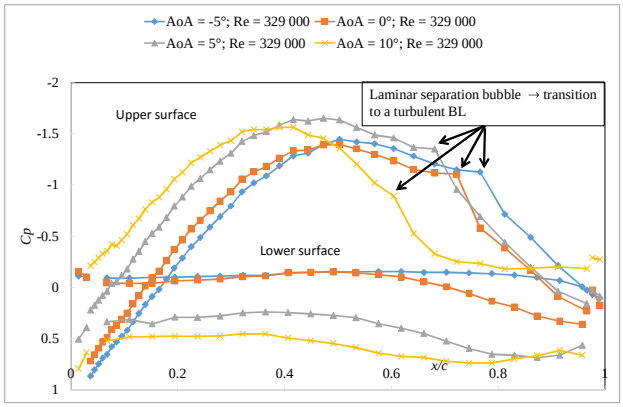

Figure 18 *Cp* distribution for high Re ≥ 226,000 and low $\alpha \leq$ 10°, versus *x/c*

The presence of the plateaus (identified by the arrows) in the downstream sections of the top surface pressure gradients is due to the presence of laminar separation bubbles (LSB). The boundary layers, which at first are laminar, separate from the profile when the adverse pressure gradient becomes too strong. When the Reynolds number is high enough, the flow transitions to turbulent and reattaches to the top face as a strong turbulent boundary layer.

The change in shape of the pressure distributions for low angles of incidence from low to high Reynolds numbers confirms that transition on the surface is due to transition

in the boundary layer. The transition, when a LSB exists, occurs at the edge of the plateau (see Figure 3). This transition occurs at x/c = 0.77 for α = -5°. When the angle of attack is increased, the stagnation point moves closer to the leading edge. Thus the flow on the top surface has more time to speed up, leading to an earlier transition. Therefore, the transition moves forward as the angle of attack is increased.

For α = -5°, the flow does not separate from the top surface before reaching the trailing edge. For increased α, a positive pressure can be seen at the trailing edge for angles from 0° to 5°. AT α = 10° the configuration is close to the ideal angle of attack, as the pressure on the top surface tends to zero when approaching the leading edge. This occurs at ideal incidence when the flow attaches tangentially to both faces. For this angle, transition has moved forward significantly, and occurs at x/c = 0.6. The LSB is very small, and the adverse pressure gradient is too strong for the turbulent boundary layer to stay attached for as long as it was for the smaller angles of incidence. Thus the flow separates at around x/c = 0.7 even when the boundary layer is turbulent.

These pressure distribution observations have clearly shown that this sudden change in flow behaviour at low incidences is due to transition occurring in the boundary layer on the top surface. This is also confirmed by CFD analysis [7,8,16,17].

5.3.3 All Reynolds Numbers/High Incidences

It needs to be said that the two previous flow configurations (Figures 17 and 18) are not really related to the study of downwind sails. Indeed, downwind sails operate at much larger Reynolds numbers of around 2 million and at larger incidences than ideal in order to prevent the sail from collapsing. However, the study of such profiles is useful in fields other than downwind sailing, such as biological flight, wind engineering and turbine design.

Figure 19 illustrates the pressure distributions measured at the high incidences (representative of a downwind sail). For these high incidences, greater than the ideal angle of attack, the shape of the pressure profiles do not depend on the Reynolds number.

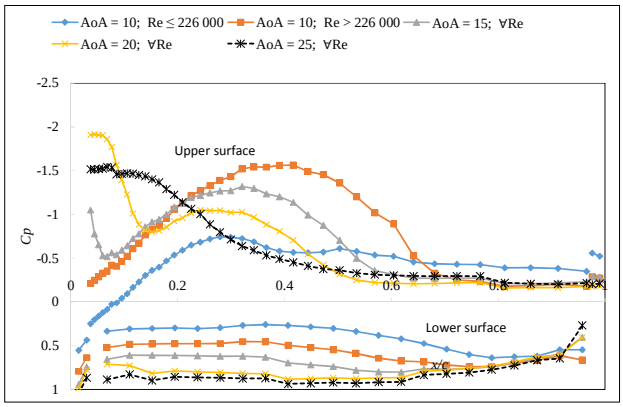

Figure 19 *Cp* distributions for high angles of incidence (α > 10°) and for all Reynolds numbers, versus x/c

Both distributions for low and high Reynolds numbers at α = 10° have been plotted in Figure 19 in order to show that whereas they are different at α = 10°, both flow regimes merge together for $\alpha \geq$ 15°. For α ≥ 15° only one single flow regime exists. The main flow characteristic that can be identified at these high incidences is the presence of a leading edge separation bubble. At angles of attack beyond ideal incidence, a leading edge bubble (LEB) is created. This occurs because the angle is too large for the flow to curve so much and to attach directly onto the profile. This bubble is characterised by a strong suction peak at the fore end of the top surface. The flow speeds up in this area. The separated shear layer, being highly unstable in this area, transitions to turbulent. It can then reattach to the top face if the angle of incidence allows it to.

The creation of this so-called leading edge bubble is thus the reason why the boundary layer is forced to be turbulent for angles of attack greater than ideal incidence. Therefore, a unique flow regime associated with the strong turbulent boundary layer can occur.

For α = 15° the leading edge bubble reattaches at around x/c = 0.06. Then the suction builds up in what is called the “recovery” area. It then separates at around x/c = 0.6. The larger the angle of attack the sooner the flow separates because of the increase in the adverse pressure gradient due to wing curvature. As the angle of attack is increased the leading edge bubble grows larger. For α = 20° it reaches a maximum of Cp = -1.9°. But as the leading edge bubble grows larger and reattaches later, the adverse pressure gradient increases as well, significantly reducing both the recovery suction magnitude and the reattachment length. For α = 25° the leading edge bubble suction reaches a smaller plateau of Cp = -1.5. As the adverse pressure gradient is even stronger, the boundary layer has no chance of recovering at all. The suction decreases slowly until it separates somewhere around x/c = 0.4.

5.4 COMPARISON WITH 3D SAILS

Finally the pressure distributions can be compared to those of a 3D model spinnaker tested in the same wind tunnel at the University of Auckland and described by Bot, et al. [19]. The pressure distributions illustrated in Figure 20 were measured at mid-height where the rigid spinnaker had a camber of 23%. The angle of attack of this section was estimated geometrically to be around 10° for an apparent wind angle of 51° and around 20° for an apparent wind angle of 59°.

The pressure distributions measured on the 2D model in the present study are very similar to those shown in Figure 20 for the 3D rigid sail. The same pressure distribution features can be identified on the 2D profile for these angles of attack. A strong leading edge bubble is followed by a suction recovery area before separating from the foil between 0.5 and 0.8 of the chord.

However, the 3D sail had its maximum camber further forward than the 2D circular arc wing model. This has the effect of moving the high suction forward in comparison to the circular arc which has its maximum camber at mid-chord.

The sail pressure distribution for AWA = 51° (blue dashed line), for which the estimated angle of attack was of around 10°, presents a very interesting feature. This angle of attack was estimated to be the ideal incidence in the present study. Indeed, at x/c = 0.6 a small plateau indicates the presence of a laminar separation bubble. The leading edge bubble in this configuration was very small. The presence of this laminar separation bubble indicates that the boundary layer is first laminar and then transitions to turbulent. For the 2D studied model at α = 10°, the laminar separation bubble occurred at exactly the same distance from the leading edge at x/c = 0.6.

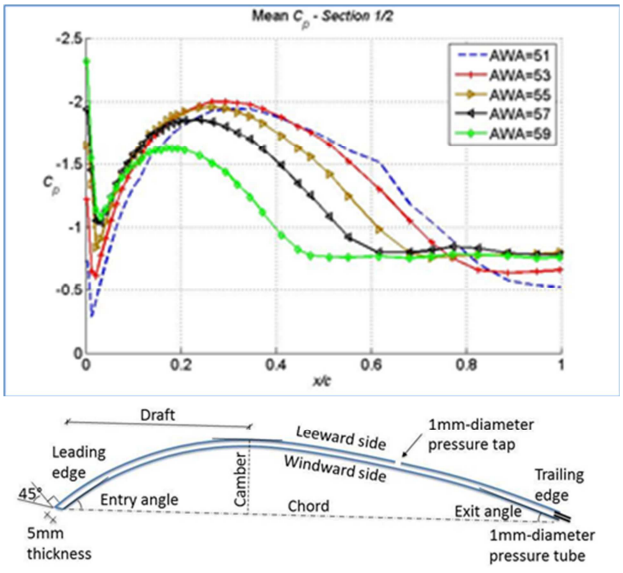

Figure 20 Pressure distributions on a spinnaker at mid-height (23% camber) (top); section geometry of the studied sail (bottom) [19]

It should be kept in mind that Reynolds numbers for sailing yachts (such as the IACC) are around 2 to 3 million. In this range of Reynolds numbers the flow will transition very close to the leading edge at ideal incidence. In practice spinnakers are used at incidences slightly greater than the ideal angle of incidence to prevent the sail from collapsing on itself or curling too much. Thus a significant leading edge bubble is expected to occur on the suction side forcing the boundary layer to be turbulent, although a spinnaker is never completely static and so such bubbles are expected to grow and collapse as the leading edge curls.

For wind tunnel testing this phenomena has to be known and controlled. Indeed a model tested at too low a Reynolds number and too low an angle of attack might produce the behaviour of a weak boundary layer with an early separation. This would provide results that actually do not represent at all what happens on a full-scale sail.

6 CONCLUSIONS

This study has allowed us to get a much clearer understanding of the flow behaviour past a thin highly cambered circular arc. The experiments were carried out in the University of Auckland Wind Tunnel for angles of attack from α = -5° to α = 25° and for a range of Reynolds numbers from Re = 116 000 to Re = 415 000.

It is evident that for angles of incidence below the ideal angle, the flow behaviour is strongly dependent on the Reynolds number. Indeed, for low Reynolds numbers the lift is initially rather low (sometimes even slightly negative) and the drag is high, while for high Reynolds numbers the lift suddenly increases and the drag drops. This transition happens very rapidly and was located between Re = 226 000 and 249 000 in the wind tunnel experiments.

CFD analysis and pressure distribution measurements have clearly shown that this sudden change in flow behaviour is due to a transition in the boundary layer on the top surface.

For low Reynolds numbers (Re $\leq$ 226 000) the flow attaches onto the top face as a laminar boundary layer. This weak boundary layer does not have enough time to transition to turbulent. Thus, being too weak to overcome the adverse pressure gradient it separates very early from the profile at around half the chord. The massive separation creates an extensive wake, creating a very small lift and a significant drag, typical of a bluff body.

On the other hand, for high Reynolds numbers (Re $\geq$ 249,000) the flow, which still attaches on the top face as a laminar boundary layer, transitions to turbulent before

separating. These transitions are easily spotted in the pressure distributions due to the typical "plateau" they create in an adverse pressure gradient region (pressure increasing due to wing curvature). The turbulent boundary layer, being fuller, stays attached much longer, thus reducing the size of the wake, and thus also reducing the drag. Furthermore, the suction region is significantly increased in both length and magnitude. This transition of the boundary layer results in a sudden increase in lift and a drop in the drag more typical of a streamlined lifting body.

For incidences higher than the ideal incidence (when the flow attaches perfectly tangentially to the top surface) a leading edge bubble is created. This bubble forces the boundary layer to be turbulent immediately the flow reattaches to the profile. Therefore, irrespective of the Reynolds number, the boundary layer is never laminar. Therefore, transition will not occur at these angles of incidence. The turbulent boundary layer still provides a strong suction. Since increasing the angle of attack also increases the adverse pressure gradient, the flow separates closer and closer to the leading edge. While the generated lift is almost constant for these angles, the drag starts to increase very rapidly.

The results from the wind tunnel have shown excellent correlations with the pressure distributions obtained for a 3D model sail. The results have been compared with the mid-height section which presented a similar camber. This indicates that even such a simplified 2D geometry as the circular arc studied yields the same flow features as for a 3D sail. Therefore, it validates the consistency of studying 2D simplified shapes as a mean of understanding more complex 3D sails, which was the original objective of studying this particular circular arc shape, formulated by the Sailing Fluids collaborators at one of their meetings.

Finally, this project has enabled us to create an extensive and accurate set of measurements for this highly cambered thin circular arc aerofoil. The goal is now for future work to use these experimental data in order to validate CFD codes for downwind sails.

REFERENCES

1. WHITE, F.M., 'Fluid Mechanics', *8th edn,. New York, McGraw-Hill,* 2016.
2. LISSAMAN, P.B.S., 'Low Reynolds number airfoils. Pasadena', *AeroVironment Inc*., 1983.
3. BRENDEL, M. AND MUELLER, T.J., 'Boundary layer measurements on an airfoil at a low Reynolds number in an oscillating freestream', *AIAA Journal, No. 3, Vol. 26. pp. 257-263,* 1988
4. MCARTHUR, J., 'Aerodynamics of wings at low Reynolds numbers: boundary layer separation and reattachment', *PhD Thesis, Aerospace Engineering, University of Southern California*, 2008.
5. SPERANZA, N., 'Development of an integrated approach for airfoil fluid dynamics', *Master's thesis, University of Rome "Tor Vergata", Italy.* July 2013.
6. BRUINING, A., 'Aerodynamic characteristics of a curved plate airfoil section at Reynolds numbers 60,000 and 100,000 and angles of attack from -10 to +90 degrees', *Delft University of Technology, Department of Aerospace Engineering, Report LR-281*, 1979.
7. COLLIE, S., JACKSON, P. AND GERRITSEN, M., 'Validation of CFD methods for downwind sail design', *High performance yacht design conference, Auckland, New Zealand,* 4-6 December, 2002.
8. COLLIE, S.J., JACKSON, P.S., GERRITSEN, M. AND FALLOW, J.B., 'Two-dimensional CFD-based parametric analysis of downwind-sail designs', *The International Journal of Small Craft Technology 146(b1),* January 2004.
9. COLLIE, S., 'Application of computational fluid dynamics to two-dimensional downwind sail flows', *PhD Thesis, University of Auckland, Auckland, New Zealand* 2006.
10. LEBRET, C., 'High cambered thin profile study', *Internship report, IRENav, Brest, France,* 2013.
11. LEBRET, C., 'Dramatic Reynolds effects on a highly cambered thin profile', *Report AB1-789, IRENav*, 2012.
12. LOMBARDI, A., 'Experimental analysis of a highly-cambered thin profile', *MSc Thesis, Department of Naval Architecture, Ocean & Marine Engineering, University of Strathclyde,* August 2014.
13. MARTIN, V., 'Reynolds number and angle of attack effects on a highly cambered thin profile's flow topology', *Report AB1-148, IRENav,* 2015.
14. THOMAS G., 'Flow phenomenology around a highly cambered thin profile. Master's thesis', *Sciences de la Mer et du Littoral Mention, Universite de Bretagne Occidentale, Brest, France,* 2015.
15. BOT, P., RABAUD, M., THOMAS, G., LOMBARDI, A., LEBRET, C., 'Sharp transition in the lift force of a fluid flowing past nonsymmetrical obstacles: evidence for a lift crisis in the drag crisis regime', *Physical Review Letters, 117, 234501,* 2016.
16. NAVA, S., BOT, P., CATER, J., NORRIS, S.E., 'Modelling the lift crisis of a cambered plate at 0° angle of attack', *Proc. Of the 20th Australasian Fluid Mechanics Conference, Perth, Australia*, 5-8 December 2016.
17. PIARD, A., 'Highly cambered thin circular arc aerofoil aerodynamics', *Master of Engineering Studies in Yacht Engineering Research Report,* July 2016.
18. VIOLA, I.M. AND FLAY, R.G.J., 'Sail pressures from full-scale, wind–tunnel and numerical investigations', *Ocean Engineering, Vol. 38, 1733-1743,* 2011
19. BOT, P., VIOLA I.M., FLAY, R.G.J., BRETT, J-S., 'Wind-tunnel pressure measurements on model-scale rigid downwind sails', *Ocean Engineering, Vo. 90. Elsevier*, 2014.

AUTHORS BIOGRAPHIES

Richard G.J. Flay, BE(Hons), PhD, is Professor of Mechanical Engineering and Director of the Yacht Research Unit in the Department of Mechanical Engineering at the University of Auckland. He has had a longstanding research interest in the wind and sailing. Since 1984 he has worked at the University of Auckland, and in 1994 he designed the World's first Twisted Flow Wind Tunnel.

Arthur Piard is a mechanical engineer working in a naval design office in France. He graduated from the University of Auckland with a Master's degree in Yacht Engineering in 2016, and from the Arts et Métiers ParisTech University in Mechanical and Industrial Engineering in 2017.

Patrick Bot, PhD, is associate Professor of Fluid Mechanics at the Naval Academy Research Institute in fluid mechanics and energy engineering. His research interests include yacht dynamics, sail aerodynamics and fluid structure interaction. His previous experience includes hydrodynamic instabilities and transition to turbulence.

.